

Probing neutrino magnetic moment at the Jinping neutrino experiment

Baobiao Yue,^a Jiajun Liao,^{*a} Jiajie Ling,^{†a,b}

^a*School of Physics, Sun Yat-sen University, No. 135, Xingang Xi Road, Guangzhou, 510275, P. R. China*

^b*Key Laboratory of Particle & Radiation Imaging (Tsinghua University), Ministry of Education, Beijing 100084, China*

E-mail: yuebb@mail2.sysu.edu.cn, liaojiajun@mail.sysu.edu.cn,
lingjj5@mail.sysu.edu.cn

ABSTRACT: Neutrino magnetic moment (ν MM) is an important property of massive neutrinos. The recent anomalous excess at few keV electronic recoils observed by the Xenon1T collaboration might indicate a $\sim 2.2 \times 10^{-11} \mu_B$ effective neutrino magnetic moment (μ_ν^{eff}) from solar neutrinos. Therefore, it is essential to carry out the ν MM searches at a different experiment to confirm or exclude such hypothesis. We study the feasibility of doing ν MM measurement with 4 kton active mass at Jinping neutrino experiment using electron recoil data from both natural and artificial neutrino sources. The sensitivity of μ_ν^{eff} can reach $1.2 \times 10^{-11} \mu_B$ at 90% C.L. with 10-year data taking of solar neutrinos. Besides the intrinsic low energy background ^{14}C in the liquid scintillator, we find the sensitivity to ν MM is highly correlated with the systematic uncertainties of pp and ^{85}Kr . Reducing systematic uncertainties (pp and ^{85}Kr) and the intrinsic background (^{14}C and ^{85}Kr) can help to improve sensitivities below these levels and reach the region of astrophysical interest. With a 3 mega-Curie (MCi) artificial neutrino source ^{51}Cr installed at Jinping neutrino detector for 55 days, it could give us a sensitivity to the electron neutrino magnetic moment (μ_{ν_e}) with $1.1 \times 10^{-11} \mu_B$ at 90% C.L.. With the combination of those two measurements, the flavor structure of the neutrino magnetic moment can be also probed at Jinping.

*Corresponding author.

†Corresponding author.

Contents

1	Introduction	1
2	νMM measurement with solar neutrinos	2
2.1	Jinping neutrino experiment	2
2.2	Solar neutrino signals	3
2.3	Background	4
2.4	Sensitivity	6
3	νMM with artificial neutrino source	9
3.1	^{51}Cr neutrino signals	9
3.2	Sensitivity	10
3.3	Combined analyses with 55-day artificial neutrino source and 10-year solar neutrinos	11
4	Conclusions	12
5	Acknowledgments	13
A	Electron scattering signal distribution and the effective neutrino flux calculation for ^{51}Cr source	16
B	An effective neutrino magnetic moment mixing $\mu_{\nu\tau}^{eff}$	18

1 Introduction

Neutrino magnetic moment (ν MM) [1–7] is related to the neutrino mass m_ν [8–13], which is verified by several neutrino oscillation experiments. Under the standard electroweak theory, it can be expressed as

$$\mu_\nu = \frac{3m_e G_F}{4\pi^2 \sqrt{2}} m_\nu \mu_B \approx 3.2 \times 10^{-19} \left(\frac{m_\nu}{\text{eV}} \right) \mu_B \quad (1.1)$$

with m_e being the electron mass, G_F the Fermi coupling constant and $\mu_B = \frac{e\hbar}{4\pi m_e}$ the Bohr magneton. The current upper bound on the neutrino masses m_ν put a constraint on μ_ν to be less than $10^{-18} \mu_B$ order. However, some theory extensions beyond MSM predict ν MM with $10^{-(10\sim 12)} \mu_B$ order [2, 14–17] for Majorana neutrino. Moreover, some general considerations [18, 19] assert that the Dirac ν MM should have a model-independent, "naturalness" upper bounds $|\mu_\nu| \lesssim 10^{-14} \mu_B$. Hence if the observation of ν MM is greater than $10^{-14} \mu_B$ [20, 21], it would be an evidence of new physics and implies that neutrino might be a Majorana particle.

A previous measurement at Super-Kamiokande reported $1.1 \times 10^{-10} \mu_B$ (90% C.L.) combined with other solar neutrino and KamLAND experiments [22]. Gemma experiment bound electron antineutrino magnetic moment ($\bar{\nu}_e \text{MM}$) below $2.9 \times 10^{-11} \mu_B$ (90% C.L.) from a reactor core with a very short baseline [23]. The Borexino collaboration reported the most stringent upper limit on μ_ν^{eff} with $2.8 \times 10^{-11} \mu_B$ (90% C.L.) [24] from solar neutrinos.

Recently, Xenon1T observed a 3σ event excess [25] at low electron recoil energies, which could be caused by νMM ($\mu_\nu^{\text{eff}} \in (1.4, 2.8) [\times 10^{-11} \mu_B]$ (90% C.L.)) from mainly pp neutrinos. In the meanwhile, PandaX-II sets an upper bound of $3.2 \times 10^{-12} \mu_B$ [26], which does not reach the possible region of νMM in Xenon1T. However, no current terrestrial experiments can validate the νMM that is suggested by Xenon1T. On the other hand, for astrophysical observations, more stringent bounds are given down to $2 \times 10^{-12} \mu_B$ (90% C.L.) [27–30]. Due to large uncertainties in astrophysical measurements, more precise terrestrial experiments are needed to explore νMM at $1 \times 10^{-11} \mu_B$ level in the near future.

A high precision measurement of solar neutrinos has been proposed by the Jinping collaboration in China, aiming to obtain high precision of solar neutrinos at the sub-percentage level [31]. We explore the possibility of carrying the measurement of νMM at Jinping neutrino experiment via solar neutrinos. We also consider a MCI-scale electron capture neutrino source like mostly ^{51}Cr [32–36], which can release sub-MeV neutrinos as well for this study, as proposed by [37, 38].

The paper is organized as follows. Section 2 depicts the study on νMM measurement with the natural neutrino source. Section 3 presents the research on νMM with a specific artificial neutrino source. Conclusions are drawn in section 4.

2 νMM measurement with solar neutrinos

2.1 Jinping neutrino experiment

The Jinping neutrino experiment (Jinping) [31] aims to study MeV-scale neutrinos, including solar neutrinos, geoneutrinos and supernova neutrinos. It is located in one of the deepest underground laboratories in the world with 2400 m vertical rock-overburden shielding, leading to a much smaller cosmic-ray muon background. The target material is the water-based liquid scintillator (LS), whose Cherenkov light can indicate the direction of charged particles and scintillation light can be used for the precise energy reconstruction of the particles. The nominal energy resolution of this kind of material is nominally 500 PE/MeV. In this study we assume a 4 kton fiducial target mass with 5 kton total mass. Comparing with Borexino, Jinping has a smaller cosmic-ray and a bigger detector mass. Therefore, Jinping could obtain more remarkable results.

νMM is detected through the neutrino elastic scattering (νES) from solar neutrinos or artificial neutrino source. The cross section of νES with νMM can be expressed as

$$\frac{d\sigma}{dT_e}(T_e, E_\nu) = \underbrace{\frac{\sigma_0}{m_e} \left[g_1^2 + g_2^2 \left(1 - \frac{T_e}{E_\nu} \right)^2 - g_1 g_2 \frac{m_e T_e}{E_\nu^2} \right]}_{\sigma_{\text{SM}}} + \underbrace{\pi \frac{\alpha^2}{m_e^2} \left(\frac{\mu_\nu}{\mu_B} \right)^2 \left(\frac{1}{T_e} - \frac{1}{E_\nu} \right)}_{\sigma_{\nu \text{MM}}}. \quad (2.1)$$

The standard model (SM) cross section contains $\sigma_0 = \frac{2G_F^2 m_e^2}{\pi} \simeq 88.06 \times 10^{-46} \text{ cm}^2$ and the electron mass $m_e = 0.511 \text{ MeV}$. For ν_e and $\bar{\nu}_e$, g_1 and g_2 yields $g_1^{(\nu_e)} = g_2^{(\bar{\nu}_e)} = \frac{1}{2} + \sin^2 \vartheta_W \simeq 0.73$ and $g_2^{(\nu_e)} = g_1^{(\bar{\nu}_e)} = \sin^2 \vartheta_W \simeq 0.23$. Whereas for $\nu_{\mu,\tau}$ and $\bar{\nu}_{\mu,\tau}$, they obey $g_1^{(\nu_{\mu,\tau})} = g_2^{(\bar{\nu}_{\mu,\tau})} = -\frac{1}{2} + \sin^2 \vartheta_W \simeq -0.27$ and $g_2^{(\nu_{\mu,\tau})} = g_1^{(\bar{\nu}_{\mu,\tau})} = \sin^2 \vartheta_W \simeq 0.23$. For ν MM cross section, μ_ν^{eff} is the effective ν MM in μ_B units. The ν MM cross section from neutrino magnetic moment is proportional to $(1/T_e - 1/E_\nu)$, which leads that the measurement of ν MM significantly depends on the capacity of the detection at low energy.

2.2 Solar neutrino signals

Jinping is far from the nuclear reactor plants. Therefore, the main part of the natural neutrinos are solar neutrinos at the low energy range. The fluxes of solar neutrinos are model-dependent. Currently, the variants of the standard solar model (SSM) can be divided into two: high metallicity (HZ) and low metallicity (LZ) [39]. In the following study, we assume the HZ hypothesis with pp ($5.98(1 \pm 0.006) \times 10^{10}$), ${}^7\text{Be}$ ($4.93(1 \pm 0.06) \times 10^9$), pep ($4.93(1 \pm 0.06) \times 10^9$), CNO ($4.88(1 \pm 0.11) \times 10^8$), ${}^8\text{B}$ ($5.46(1 \pm 0.12) \times 10^6$) and hep ($7.98(1 \pm 0.30) \times 10^3$) in the unit of $\text{cm}^{-2}\text{s}^{-1}$. In this study, the contributions from pp and ${}^7\text{Be}$ neutrinos dominate the measurement of ν MM according to ref. [24]. The electron recoiling signals of Carbon-Nitrogen-Oxygen (CNO) fusion circle, pep , ${}^8\text{B}$ and hep neutrinos can be neglected with regard to the measurement of ν MM due to the small component at low energy region.

In general, the prediction of the electron scattering signal from solar neutrinos can be counted by

$$N_{pre}(T_e) = N_e T \sum_i \phi_i \int S_i^\odot(E_\nu) \sum_{\alpha=e,\mu,\tau} P_{e\alpha}^i(E_\nu) \sigma_\alpha(E_\nu, T_e) dE. \quad (2.2)$$

N_e is the total electron number of the fiducial volume counted as $N_e = V \rho_{\text{LS}} \rho_e N_A = 1.35 \times 10^{33}$ with the total volume V , T is the exposure time, the LS density ρ_{LS} , the electron density per gram ρ_e (mol/g) and the Avogadro constant N_A . i is the i^{th} solar neutrino source. ϕ_i is the corresponding neutrino flux. S_i^\odot is the normalized energy spectrum of such neutrino. $P_{e\alpha}^i(E_\nu)$ is the oscillation probability, which is weighted by the different neutrino distributions in the sun, with $e - \alpha$ flavor transition from the sun to the earth. The i^{th} $P_{e\alpha}^i(E_\nu)$ can be approximately given as

$$P_{e\alpha}^i(E_\nu) = \int_0^{R_\odot} F_i(r) P_{e\alpha}^\odot(r, E_\nu) dr, \quad (2.3)$$

where R_\odot is the radius of the sun, $F_i(r)$ is the normalized i^{th} neutrino distribution [40] as a function of r , which is the distance to the center of the sun, and $P_{e\alpha}^\odot(r, E_\nu)$ is the oscillation probability of neutrino produced at r with an energy E_ν and detected at the earth. As a good approximation, the matter effect from the earth is neglected in the night due to the very low neutrino energy of pp and ${}^7\text{Be}$ ($E_\nu^{max} < 1 \text{ MeV}$). Therefore, $P_{e\alpha}^\odot(r, E_\nu)$ takes no account of the day-night effect. σ_α is the cross section of ν ES with α -flavor neutrinos.

In this study, we assume 100% detection efficiency in the fiducial volume. Figure 1

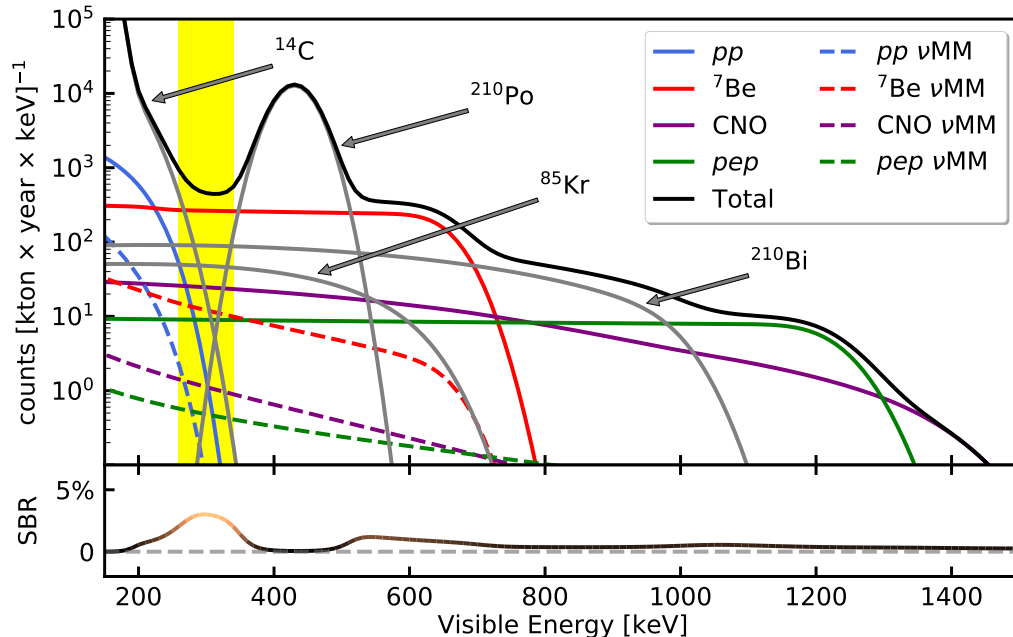


Figure 1: Events distribution with signal and background components. The dashed lines correspond to the contributions of the magnetic moment from their sources with the same color. The target signal is the electronic recoil caused by ν MM from all solar neutrinos. The SM ES signal is also background for ν MM. The yellow band represents the region with the relative large ν MM signal-to-background ratio shown in the subplot for all neutrinos, assuming $\mu_\nu^{eff} = 2.2 \times 10^{-11} \mu_B$, which is the best fit of ν MM hypothesis in Xenon1T [25].

shows the predictions of each components including signal and background. We generate the solar neutrino signal by using the parameters in PDG 2020 [41]. In order to measure ν MM precisely, it is crucial to evaluate accurately all components which are overwhelming the most sensitive ν MM detection region, the region of interest (ROI) plotted with the yellow band in this figure. For the solar neutrinos, the SM ν ES part of pp could mimic ν MM ES part of itself because of the similar spectra of them. Therefore, the external constraint of the flux of pp takes an important role. the flux of pp neutrino can be mainly limited by the radiochemical constraints with 5% from gallium experiments [42]. The electron recoil with ${}^7\text{Be}$ neutrinos rises an outstanding "shoulder" structure up from about 500 to 700 keV, providing a precise measurement of ${}^7\text{Be}$ neutrino flux. The fluxes of CNO and pep could be counted from about 900 to 1300 keV, where ν MM is negligible due to the higher neutrino energy and lower fluxes than pp and ${}^7\text{Be}$.

2.3 Background

In general, three types background should be considered: cosmic-ray muon induced background, internal radioactive background and external radioactive background. However, for ν MM study, all SM ν ES components are also kinds of background to ν MM. The rate of

cosmic-ray muon induced background can be about 200 times lower than those in Borexino due to the depth of the Jinping laboratory [31]. The main low-energy background from cosmic-ray is ^{14}C at low energy. However, it does not affect the measurement of νMM due to its high energy (> 1.5 MeV). Other cosmogenic isotopes will not be considered in this study. We assume the internal radioactive background can be reduced to the same level as Borexino Phase-II [43] after purifications. The intrinsic ^{14}C of LS is $2.7 \times 10^{-18} \text{g/g}$ in Borexino. The external γ -rays can be predicted with an exponential scale factor according to the distance from the edge of the fiducial volume to the detector surface. However, it is also insignificant because it dominates at high energy range (> 1.5 MeV). For νMM study, ^{14}C , ^{210}Bi , ^{85}Kr and ^{210}Po are the main background shown with the rate in table 1. The pile-up of ^{14}C - ^{14}C has been considered for Jinping. We assume a naive 200 ns signal window (δt) to coarsely estimate the rate as

$$R_{\text{pile-up}} \approx 2 \times \frac{(R_{^{14}\text{C}} \times M_{FV}) \times (R_{^{14}\text{C}} \times M_{TV}) \times \delta t}{M_{FV}} \approx 28000 \text{ cpd/kton}, \quad (2.4)$$

where M_{FV} is the fiducial volume mass, M_{TV} is the total volume mass and δt is the signal integral window. The spectrum of it is generated through the convolution with the spectrum of ^{14}C . Other pile-up events, mainly ^{14}C with external γ -rays and ^{210}Po with external γ -rays [44], are negligible.

Background	Rate [cpd/kton]
^{14}C	$3.456(1 \pm 0.05) \times 10^7$
^{85}Kr	$68(1 \pm 0.26)$
^{210}Bi	$175(1 \pm 0.11)$
^{210}Po	$2600(1 \pm 0.01)$

Table 1: Background rates taken from Borexino Phase-II [43].

In general, ^{14}C could be determined independently from the main analysis as Borexino suggested [45]. ^{14}C shuts down the feasibility of any signal detection at low energy due to its huge abundance below 150 keV. Thanks to the better resolution at Jinping, ^{14}C could not bury pp and ^7Be neutrinos severely above 150 keV. However, the measurement of pp is still challenging because of the pile-up of ^{14}C - ^{14}C . Optimistically, we neglect the shape uncertainty of ^{14}C [46]. ^{210}Po , overwhelming in the region of 350-550 keV, can be fitted clearly with a gaussian distribution. In addition, α particle from ^{210}Po could also be discriminated with scintillation pulse shape from e^\pm . Conservatively, ^{210}Po is still considered in this study. ^{210}Bi appears as a "shoulder" structure in the region from about 700 to 1000 keV with a relatively big event number. Therefore, ^{210}Bi could be fitted well.

Thanks to the energy resolution of Jinping experiment, there is a wide ROI, the yellow band in figure 1, between ^{14}C and ^{210}Po spectra to measure the νMM . However, ^{85}Kr hides under all other components in ROI, resulting in a difficult measurement. In addition, It could almost freely mimic the shape and rate of νMM component, especially νMM from ^7Be , in ROI of νMM . That is to say, the residual ^{85}Kr of the detector material can significantly

influence the measurement of ν MM. Therefore, the good purification and the independent measurement of ^{85}Kr could accordingly improve the capability of ν MM measurement for Jinping experiment. In general, it is uncertain the the purification of ^{85}Kr improves 1 or 2 order, according to the analysis in Borexino Phase-II [43]. Fortunately, ^{85}Kr has a rather small branch of β decay (0.4%) with a coincidence signal, which could be selected with 18% efficiency proposed by Borexino Phase-II [43], giving a 4% bound by 10-year measurement at Jinping.

2.4 Sensitivity

For the sensitivity study, we build a χ^2 function as

$$\chi^2 = \sum_i^{T_e} \frac{(N_{pre}^i - N_{obs}^i)^2}{N_{obs}^i} + \sum_{\alpha} \left(\frac{\delta_{\alpha}}{\sigma_{\alpha}}\right)^2, \quad (2.5)$$

where N_{pre}^i and N_{obs}^i are the event number in the i^{th} bin of the prediction and the observation with visible energy from 150 to 1500 keV, and $(\frac{\delta_{\alpha}}{\sigma_{\alpha}})^2$ is the penalty term to constrain solar neutrino oscillation parameters (i.e. θ_{12} and Δm_{21}^2), solar neutrino fluxes and background. In $(\frac{\delta_{\alpha}}{\sigma_{\alpha}})^2$, δ_{α} means the difference between the value of fitting parameter α and the center value of its prior and σ_{α} is 1 σ error.

Because there are multiple components, which are overlapping with each other at different visible energy regions, a simultaneous analysis method is necessary to take out all information for each part. Therefore, Markov chain Monte Carlo (MCMC) technique is used to study the correlations among multi parameters, especially the relations between ν MM and any other parameter, and to obtain the individual posterior distribution of each component simultaneously. MCMC is based on a pythonic package named emcee [47], in which a likelihood function is needed. Therefore, we convert the χ^2 function into likelihood through $\mathcal{L} = \exp(-\frac{1}{2}\chi^2)$ for MCMC.

Figure 2 presents a multi-parameter scatter plots with the full parameters by MCMC after a 10-year data taking, showing the correlations of each two parameters and the distributions of full parameters. Solar neutrino parameters are relative to the HZ fluxes: $R_{\phi^{\odot}} = \phi^{\odot}/\phi_{truth}^{\odot}$. Background parameters are the relative differences to the background truth rates in table 1: $\delta\text{BG}=(\text{BG}-\text{BG}_{truth})/\text{BG}_{truth}$. This MCMC assumes that $\sin^2\theta_{12}$ and Δm_{21}^2 is constrained by JUNO, which could have accurate measurements of $\sin^2\theta_{12}$ and Δm_{21}^2 [48] with sub-percentage of 0.54% and 0.24% respectively, and pp is constrained with 5% by Gallium experiments. The MCMC scatter plot shows that pp and ^{85}Kr have the largest correlation coefficients with μ_{ν}^{eff} . Therefore, good priors of pp or ^{85}Kr do make corresponding improvements on the detection sensitivities of μ_{ν}^{eff} as what we expected in the analyses of previous subsections. From another point of view, the existence of ν MM could bias the measurement of pp in the similar experiments. In figure 2, ^{210}Bi has very strong correlations with both CNO and pep . Therefore, we could fix CNO and pep in the following study because ^{210}Bi spectrum can mimic them in the low energy range.

Assuming 10-year exposure, we fix μ_{ν}^{eff} by different values to obtain the 90% C.L. upper limits in figure 3 by χ^2 minimizer as another tool to study the influences with different

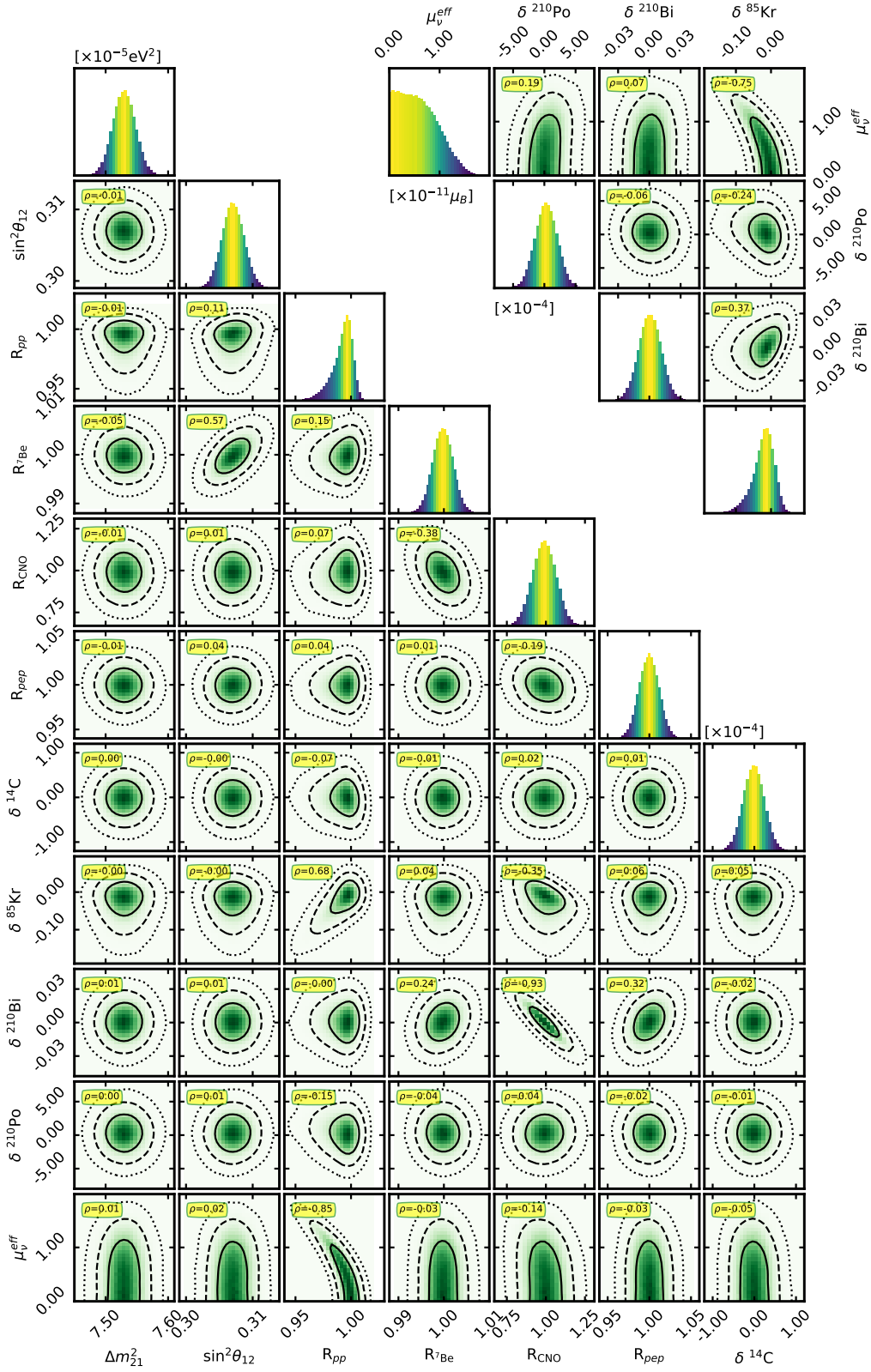


Figure 2: MCMC result with 10-year data taking. The solid, dashed and dotted lines present 1σ , 2σ and 3σ in all contours. In order to fit MCMC plot in one page, we put the lower right corner to the upper right corner.

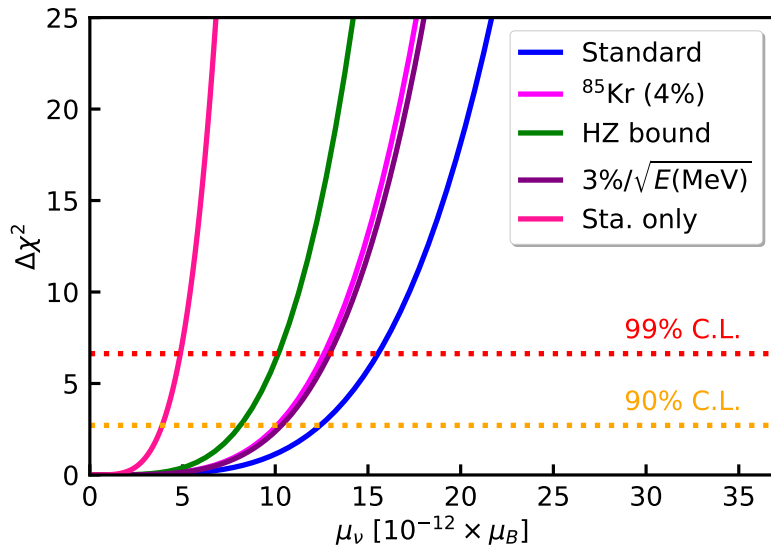


Figure 3: The 90% C.L. upper limit at Jinping. The blue line is the standard case with only the radiochemical constraints from Gallium experiments. The fuchsia line presents the standard case with additional 4% bound on ^{85}Kr . The green line means the standard case with additional HZ model flux bounds. The purple line is the standard case with 3% energy resolution. The deep pink line is the statistics only case.

cases. The sensitivities to νMM from The MCMC method and χ^2 minimizer are consistent with each other. We find that fixing $\sin^2\theta_{12}$ and Δm_{21}^2 leads no differences about the sensitivity of νMM in fitter, compared with the case that they are constrained by JUNO. The standard case assumes that $\sin^2\theta_{12}$, Δm_{21}^2 , CNO and pep are fixed, pp is bounded by Gallium experiments and other parameters are all free. In figure 3, the standard case can reach $1.2 \times 10^{-11}\mu_B$, which is much better than other natural neutrino experiments. The 4% ^{85}Kr bound can boost the 90% upper limit to $1 \times 10^{-11}\mu_B$ as well as $3\%/\sqrt{E(\text{MeV})}$, high light yield LS. Moreover, HZ flux bound, particularly pp and ^7Be fluxes, can also improve a lot, leading to the νMM bound down to $0.8 \times 10^{-11}\mu_B$. The most ambitious sensitivity one is the statistics-only case with $3.9 \times 10^{-12}\mu_B$ level at 90% C.L. for the case of such background level in table 1. If the background level could reduced, the result will get better.

With naive background reductions, we calculate the sensitivity to νMM with different individual reductions of ^{14}C , ^{85}Kr , ^{210}Po and ^{210}Bi . We find that the reductions of ^{14}C and ^{85}Kr could significantly improve the sensitivity to νMM . It would take a more than 10,000-fold reduction in ^{14}C background to reach $1.0 \times 10^{-12}\mu_B$ level. A more than 1000-fold reduction in ^{85}Kr background could at most reach $6.0 \times 10^{-12}\mu_B$ level. More reduction in ^{85}Kr could not improve any sensitivity. Any reduction of ^{210}Po and ^{210}Bi could hardly improve the sensitivity to νMM . We also find that Jinping has more than 5σ (3σ) to confirm or exclude the νMM hypothesis about the recent excess in Xenon1T in 10 years (4

years).

3 ν MM with artificial neutrino source

3.1 ^{51}Cr neutrino signals

As a specific example, a 3 MCi initialized ^{51}Cr source [38] is assumed to be placed outside with 1 meter away from the edge of the fiducial volume or inside at the center of the detector with shielding. Figure 4 shows the cartoon sketch of the proposed source positions. The decay of ^{51}Cr is $^{51}\text{Cr} + e^- \rightarrow ^{51}\text{V} + \nu_e$, with a 27.7-day half-life. The monoenergetic neutrino energies are 752 keV (9%), 747 keV (81%), 432 keV (1%) and 427 keV (9%) respectively.

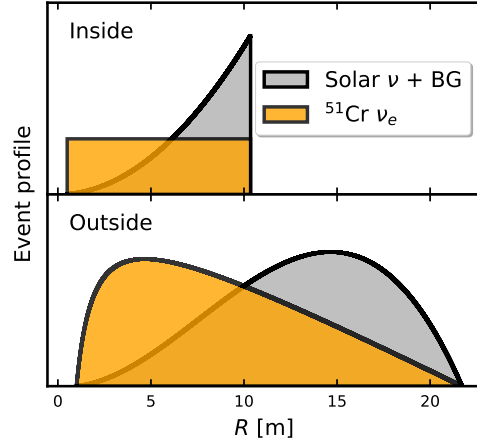
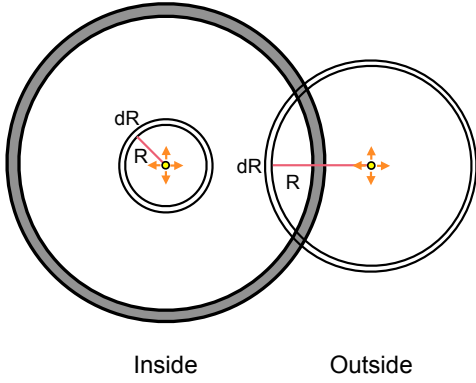


Figure 4: The cartoon sketch about the source positions. The sizes of them are not proportional to the actual sizes. **Figure 5:** The normalized event profile with respect to R from the source.

We calculate event vertex distribution as the function of R , which is the distance from the event position to the artificial source for both cases and the event number based on appendix A. Figure 5 presents the event profile in the different slices as a function of R , assuming an ideal reconstruction performance. The position information can provide a strong capability to separate the signal of ^{51}Cr and the almost uniform solar neutrinos and background in the fiducial volume. We obtain the effective neutrino fluxes relative to the solar neutrino with 55-day ^{51}Cr source for both cases as

$$\phi_{eff} = \begin{cases} 1.27 \times 10^{10} \text{ [cm}^{-2}\text{s}^{-1}] & \text{(Inside)} \\ 4.79 \times 10^9 \text{ [cm}^{-2}\text{s}^{-1}] & \text{(Outside)} \end{cases} . \quad (3.1)$$

Considering both cases, we simulate the signal and background as shown in figure 6. For solar neutrino, the event contains the ν MM contribution from ν_e , ν_μ and ν_τ . However,

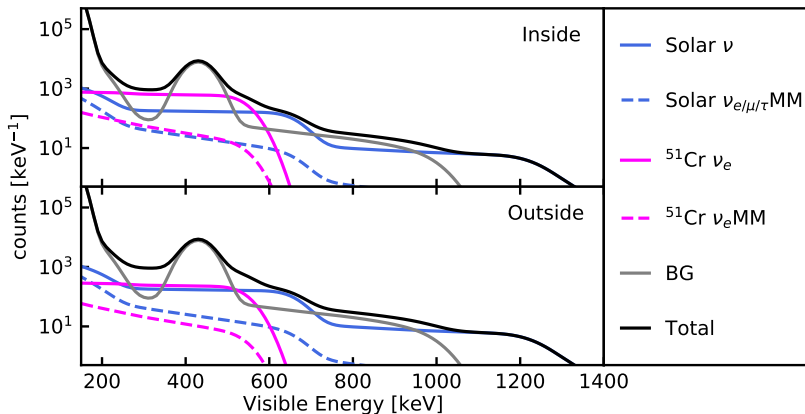


Figure 6: The event number of each component by 55-day data taking with the assumption $(\mu_{\nu_e}, \mu_{\nu_\mu}, \mu_{\nu_\tau}) = (3.9, 5.8, 5.8) [\times 10^{-11} \mu_B]$, the individual 90% C.L. upper limits at Borexino [24].

the source can only contribute the ν_e MM. Therefore, the artificial neutrino source signal can significantly break the structure of ν_e , ν_μ and ν_τ magnetic moment in solar neutrinos, which has been presented in [24, 49], when combined with solar neutrino signal. In this case, the probing of ν_e MM will be robuster than the others.

In figure 6, ^{51}Cr shows a outstanding "shoulder" structure between 500 and 600 keV, where the flux of ^{51}Cr could be counted precisely. Moreover, the amount of ν_e MM shown as dash line in blue color from ^{51}Cr source is almost equal to the summation of ν_e MM, ν_μ MM and ν_τ MM shown as dash line in fuchsia color from solar neutrinos for both cases. That is to say, the sensitivity to ν_e MM should be better than other neutrino flavor magnetic moment. The ROI of ν MM with ^{51}Cr source is the same as the solar-only case in figure 1.

3.2 Sensitivity

We build a similar χ^2 function as eq. (2.5) to study μ_{ν_e} , μ_{ν_μ} , μ_{ν_τ} separately. We find that $T_e - R$ (visible energy and event vertex by R) two dimensional fit is almost equal $T_e - R - T$ (visible energy, event vertex by R and time) three dimensional fit. However, T_e (visible energy) one dimensional fit gets much worse sensitivity than others. Therefore, we adopt the 2 dimensional χ^2 function in the following study as

$$\chi^2 = \sum_i^{T_e} \sum_j^R \frac{(N_{pre}^{i,j} - N_{obs}^{i,j})^2}{N_{obs}^{i,j}} + \sum_\alpha \left(\frac{\delta_\alpha}{\sigma_\alpha}\right)^2, \quad (3.2)$$

where i is the i^{th} T_e bin from 150 to 1500 keV, j is the j^{th} reconstructed R bin. Compared with section 2, the fitter has an extra parameter, the flux of ^{51}Cr ν_e . We bound it within 1% in the following analyses. And other parameters are consistent with the standard case in section 2.

Figure 7 presents the individual results about ν MM with different flavors. Obviously, μ_{ν_e} gets the most stringent constraint among all neutrino flavors due to the strong ν_e source.

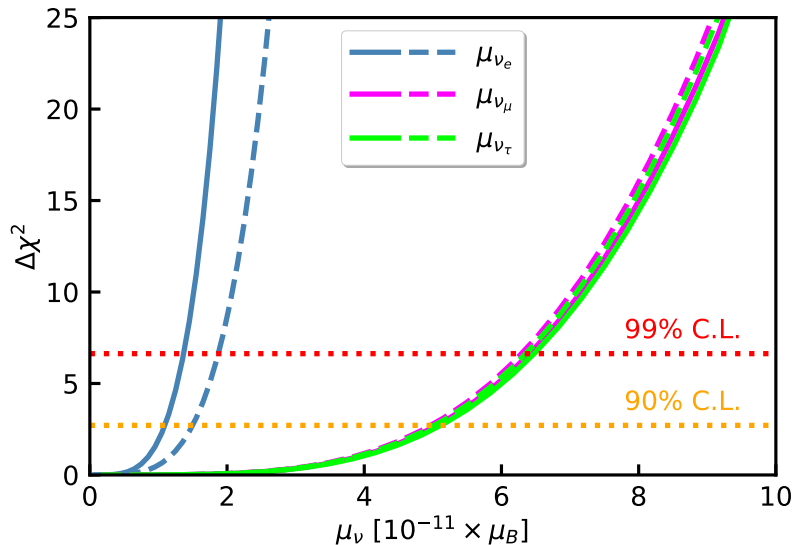


Figure 7: The sensitivity with each ν MM components using 55-day data taking. The solid (dash) lines represent the inside (outside) ^{51}Cr case.

90% C.L./ $[\times 10^{-11} \mu_B]$	μ_{ν_e}	μ_{ν_μ}	μ_{ν_τ}
Inside ^{51}Cr	1.1	5.1	5.1
Outside ^{51}Cr	1.5	5.0	5.0

Table 2: 90% C.L. upper limits of ν MM with 55-day data taking.

When assuming the inside case, μ_{ν_e} gets more tightly bounded than the outside case on account of more electron recoil event from the source. However, the bounds on μ_{ν_μ} and μ_{ν_τ} from solar neutrinos become a little weaker because ^{51}Cr ν_e affects as a kind of background for μ_{ν_μ} and μ_{ν_τ} . With 55-day data taking, we obtain the results with 90% C.L. upper limits shown in table 2. If we reduce the systematic uncertainties (pp and ^{85}Kr) and the intrinsic background (^{14}C and ^{85}Kr) and enrich the strength of ^{51}Cr source, we will obtain better results.

3.3 Combined analyses with 55-day artificial neutrino source and 10-year solar neutrinos

10-year data taking of solar neutrinos could give a stringent bound on μ_ν^{eff} with the combination of μ_{ν_e} , μ_{ν_μ} and μ_{ν_τ} . And 55-day data taking of ^{51}Cr could make a tighter limit on μ_{ν_e} . To reach a better sensitivity, we combine them with 10-year solar neutrinos and 55-day ^{51}Cr source neutrinos. We define a mixing of μ_{ν_μ} and μ_{ν_τ} , i.e. $\mu_{\nu_{\mu\tau}}^{eff}$, which presents the mixing of ν_μ and ν_τ in solar neutrinos. An approximate mixing $\left(\mu_{\nu_{\mu\tau}}^{eff}\right)^2 \simeq 0.49\mu_{\nu_\mu}^2 + 0.51\mu_{\nu_\tau}^2$ is obtained from the appendix B.

The left plot of figure 8 shows the 2 dimensional 90% C.L. contours with respect to μ_{ν_e}

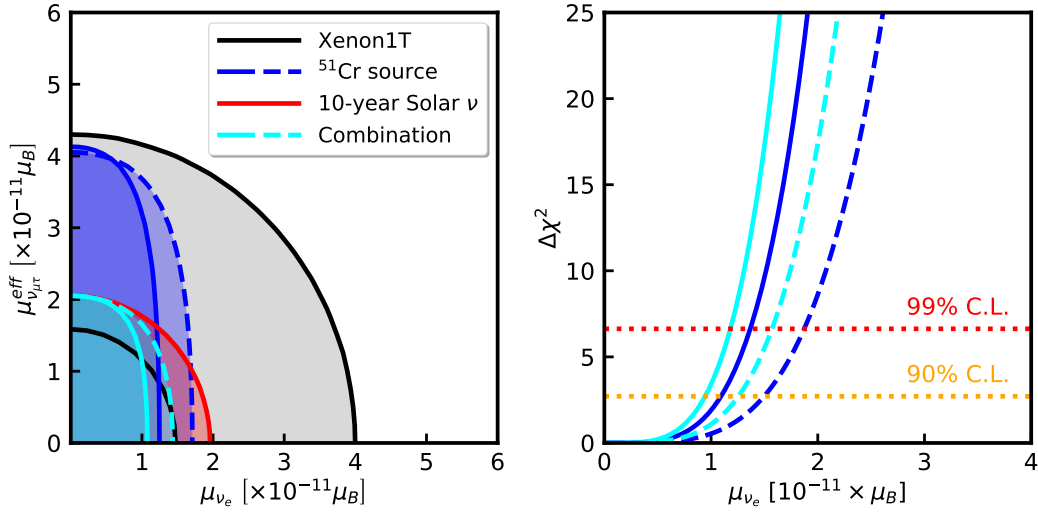


Figure 8: The left plot is the 90% C.L. upper limits in μ_{ν_e} and $\mu_{\nu_{\mu\tau}}^{eff}$ plane corresponding to different cases. And the right one is the marginalizations by μ_{ν_e} . The gray band is the possible area with 90% C.L. in Xenon1T. The solid (dash) lines represent the inside (outside) ^{51}Cr case. The combination means that 10-year solar data plus 55-day ^{51}Cr neutrino source.

and $\mu_{\nu_{\mu\tau}}^{eff}$ plane. We reproduce the Xenon1T access with 90% C.L. band in μ_{ν_e} and $\mu_{\nu_{\mu\tau}}^{eff}$ plane to compare with this study. With a ^{51}Cr source, the constraint on μ_{ν_e} boosts a lot. It is even more stringent than 10-year solar data taking. 55-day ^{51}Cr could exclude almost all possible parameter space, especially ν_e space, in that plane. And 10-year solar neutrino could also exclude a lot possible parameter space. The right plot of figure 8 presents the marginalization by μ_{ν_e} , showing the combination could weakly boost μ_{ν_e} to $0.9 \times 10^{-11} \mu_B$ ($1.3 \times 10^{-11} \mu_B$) for inside case (outside case).

4 Conclusions

νMM measurement plays an important role in determining the intrinsic nature of neutrinos and probing new physics in the neutrino sector. The νMM has been constrained to the $3 \times 10^{-11} \mu_B$ level at 90% C.L. by many terrestrial neutrino experiments. However, Xenon1T recently reports a hint of a $2.2 \times 10^{-11} \mu_B$ effective neutrino magnetic moment. We have calculated the feasibility of doing νMM measurement at Jinping neutrino experiment with both natural and artificial neutrino sources.

We find the sensitivity of μ_{ν}^{eff} can reach $1.2 \times 10^{-11} \mu_B$ level at 90% C.L. with 10-year solar neutrino data taking at Jinping, which can validate the νMM hypothesis in Xenon1T by more than 5σ . A 4% bound on ^{85}Kr or 3% energy resolution could improve the sensitivity to $1.0 \times 10^{-11} \mu_B$. The HZ model flux bound on pp and ^7Be could lead to $0.8 \times 10^{-11} \mu_B$ at 90% C.L.. We find that more than 10,000-fold reduction of ^{14}C and

1000-fold reduction of ^{85}Kr could improve the result to the $1 \times 10^{-12} \mu_B$ and $0.6 \times 10^{-11} \mu_B$ respectively. The statistics-only result for the νMM is $0.4 \times 10^{-11} \mu_B$.

With respect to 3 MCi ^{51}Cr neutrino source, $\nu_e\text{MM}$ can be measured with $1.1 \times 10^{-11} \mu_B$ ($1.5 \times 10^{-11} \mu_B$) at 90% C.L. for inside (outside) the detector in 55 days. We have also considered the combination of 10-year solar neutrino and 55-day ^{51}Cr to determine the neutrino magnetic moment induced by different neutrino flavors.

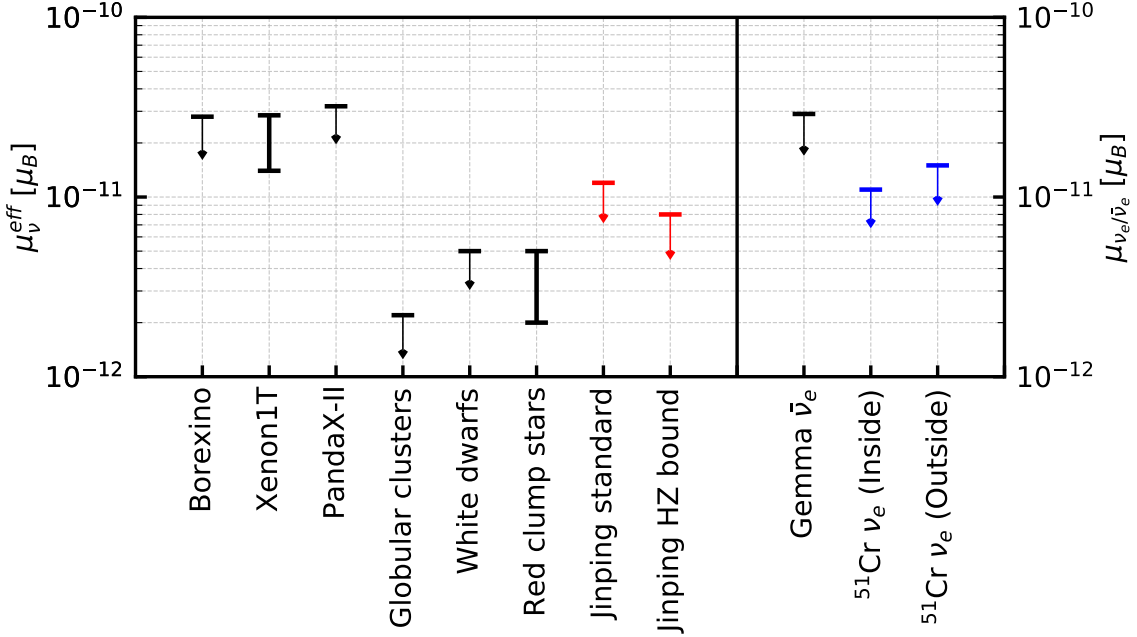


Figure 9: The current status (90% C.L.) of the neutrino magnetic moment and the sensitivities of Jinping both with solar neutrinos and artificial source.

In the end, we present the current results of νMM and the sensitivities of both solar neutrino and artificial neutrino sources at Jinping in figure 9. The left segment of figure 9 shows μ_ν^{eff} from this work compared to terrestrial experiments: Borexino [24], Xenon1T [25] and PandaX-II [26], also with the astrophysical observations: cooling of globular clusters [29], white dwarfs [30] and red clump stars [50]. The right segment presents the electronic neutrino magnetic moment from this work with ^{51}Cr source compared to Gemma experiment [23]. Jinping could validate the νMM that is suggested by Xenon1T in the future. It could reach the region of astrophysical interest by reducing the systematic uncertainties and the intrinsic background or by enriching the strength of ^{51}Cr source.

5 Acknowledgments

Jiajie Ling acknowledges the support from National Key R&D program of China under grant NO. 2018YFA0404013, National Natural Science Foundation of China under Grant NO. 11775315, Key Lab of Particle & Radiation Imaging, Ministry of Education. Jiajun Liao acknowledges the support from the National Natural Science Foundation of China

(Grant No. 11905299), Guangdong Basic and Applied Basic Research Foundation (Grant No. 2020A1515011479), the Fundamental Research Funds for the Central Universities, and the Sun Yat-Sen University Science Foundation.

During preparing this paper, we notice an independent and similar study [[arXiv:2103.11771](https://arxiv.org/abs/2103.11771)] is also proposed and studied by Z. Ye *et al.* simultaneously.

References

- [1] L. Okun, M. Voloshin and M. Vysotsky, *Electromagnetic Properties of Neutrino and Possible Semiannual Variation Cycle of the Solar Neutrino Flux*, *Sov. J. Nucl. Phys.* **44** (1986) 440.
- [2] L. Okun, M. Voloshin and M. Vysotsky, *Neutrino Electrodynamics and Possible Effects for Solar Neutrinos*, *Sov. Phys. JETP* **64** (1986) 446.
- [3] C.-S. Lim and W.J. Marciano, *Resonant Spin - Flavor Precession of Solar and Supernova Neutrinos*, *Phys. Rev. D* **37** (1988) 1368.
- [4] E.K. Akhmedov, *Resonant Amplification of Neutrino Spin Rotation in Matter and the Solar Neutrino Problem*, *Phys. Lett. B* **213** (1988) 64.
- [5] H. Back et al., *Study of the neutrino electromagnetic properties with prototype of Borexino detector*, *Phys. Lett. B* **563** (2003) 35.
- [6] W. Grimus, M. Maltoni, T. Schwetz, M. Tortola and J. Valle, *Constraining Majorana neutrino electromagnetic properties from the LMA-MSW solution of the solar neutrino problem*, *Nucl. Phys. B* **648** (2003) 376 [[hep-ph/0208132](https://arxiv.org/abs/hep-ph/0208132)].
- [7] C. Giunti and A. Studenikin, *Neutrino electromagnetic interactions: a window to new physics*, *Rev. Mod. Phys.* **87** (2015) 531 [[1403.6344](https://arxiv.org/abs/1403.6344)].
- [8] K. Fujikawa and R. Shrock, *The Magnetic Moment of a Massive Neutrino and Neutrino Spin Rotation*, *Phys. Rev. Lett.* **45** (1980) 963.
- [9] J. Schechter and J. Valle, *Majorana Neutrinos and Magnetic Fields*, *Phys. Rev. D* **24** (1981) 1883.
- [10] B. Kayser, *Majorana Neutrinos and their Electromagnetic Properties*, *Phys. Rev. D* **26** (1982) 1662.
- [11] J.F. Nieves, *Electromagnetic Properties of Majorana Neutrinos*, *Phys. Rev. D* **26** (1982) 3152.
- [12] P.B. Pal and L. Wolfenstein, *Radiative Decays of Massive Neutrinos*, *Phys. Rev. D* **25** (1982) 766.
- [13] R.E. Shrock, *Electromagnetic Properties and Decays of Dirac and Majorana Neutrinos in a General Class of Gauge Theories*, *Nucl. Phys. B* **206** (1982) 359.
- [14] M. Fukugita and T. Yanagida, *A Particle Physics Model for Voloshin-Vysotskii-Okun Solution to the Solar Neutrino Problem*, *Phys. Rev. Lett.* **58** (1987) 1807.
- [15] S. Pakvasa and J. Valle, *Neutrino properties before and after KamLAND*, *Proc. Indian Natl. Sci. Acad. A* **70** (2004) 189 [[hep-ph/0301061](https://arxiv.org/abs/hep-ph/0301061)].
- [16] M. Gorchtein, N.F. Bell, M.J. Ramsey-Musolf, P. Vogel and P. Wang, *Model Independent Naturalness Bounds on Magnetic Moments of Majorana Neutrinos*, *AIP Conf. Proc.* **903** (2007) 287 [[hep-ph/0610388](https://arxiv.org/abs/hep-ph/0610388)].

- [17] N.F. Bell, M. Gorchtein, M.J. Ramsey-Musolf, P. Vogel and P. Wang, *Model independent bounds on magnetic moments of Majorana neutrinos*, *Phys. Lett. B* **642** (2006) 377 [[hep-ph/0606248](#)].
- [18] N.F. Bell, V. Cirigliano, M.J. Ramsey-Musolf, P. Vogel and M.B. Wise, *How magnetic is the Dirac neutrino?*, *Phys. Rev. Lett.* **95** (2005) 151802 [[hep-ph/0504134](#)].
- [19] N.F. Bell, V. Cirigliano, M. Ramsey-Musolf, P. Vogel and M.B. Wise, *Magnetic moments of Dirac neutrinos*, *AIP Conf. Proc.* **842** (2006) 874 [[hep-ph/0601005](#)].
- [20] B. Kayser, *Neutrino properties*, *Proc. of "The Neutrino 08"*, Christchurch, New Zealand, May 25-31 (2008) .
- [21] C. Giunti and A. Studenikin, *Neutrino electromagnetic properties*, *Phys. Atom. Nucl.* **72** (2009) 2089 [[0812.3646](#)].
- [22] BOREXINO collaboration, *Direct Measurement of the Be-7 Solar Neutrino Flux with 192 Days of Borexino Data*, *Phys. Rev. Lett.* **101** (2008) 091302 [[0805.3843](#)].
- [23] A.G. Beda, V.B. Brudanin, V.G. Egorov, D.V. Medvedev, V.S. Pogosov, E.A. Shevchik et al., *Gemma experiment: The results of neutrino magnetic moment search*, *Physics of Particles and Nuclei Letters* **10** (2013) 139.
- [24] BOREXINO collaboration, *Limiting neutrino magnetic moments with Borexino Phase-II solar neutrino data*, *Phys. Rev. D* **96** (2017) 091103 [[1707.09355](#)].
- [25] XENON collaboration, *Excess electronic recoil events in XENON1T*, *Phys. Rev. D* **102** (2020) 072004 [[2006.09721](#)].
- [26] PANDAX-II collaboration, *A search for solar axions and anomalous neutrino magnetic moment with the complete PandaX-II data*, [2008.06485](#).
- [27] G.G. Raffelt, *Core Mass at the Helium Flash From Observations and a New Bound on Neutrino Electromagnetic Properties*, *Astrophys. J.* **365** (1990) 559.
- [28] S. Arceo-Díaz, K.-P. Schröder, K. Zuber and D. Jack, *Constraint on the magnetic dipole moment of neutrinos by the tip-RGB luminosity in ω -Centauri*, *Astropart. Phys.* **70** (2015) 1.
- [29] S.A. Díaz, K.-P. Schröder, K. Zuber, D. Jack and E.E.B. Barrios, *Constraint on the axion-electron coupling constant and the neutrino magnetic dipole moment by using the tip-RGB luminosity of fifty globular clusters*, [1910.10568](#).
- [30] A.H. Córscico, L.G. Althaus, M.M. Miller Bertolami, S. Kepler and E. García-Berro, *Constraining the neutrino magnetic dipole moment from white dwarf pulsations*, *JCAP* **08** (2014) 054 [[1406.6034](#)].
- [31] JINPING collaboration, *Physics prospects of the Jinping neutrino experiment*, *Chin. Phys. C* **41** (2017) 023002 [[1602.01733](#)].
- [32] J. Abdurashitov et al., *Measurement of the response of a Ga solar neutrino experiment to neutrinos from an Ar-37 source*, *Phys. Rev. C* **73** (2006) 045805 [[nucl-ex/0512041](#)].
- [33] GALLEX collaboration, *Final results of the Cr-51 neutrino source experiments in GALLEX*, *Phys. Lett. B* **420** (1998) 114.
- [34] SAGE collaboration, *Measurement of the response of the Russian-American gallium experiment to neutrinos from a Cr-51 source*, *Phys. Rev. C* **59** (1999) 2246 [[hep-ph/9803418](#)].

- [35] M. Cribier et al., *Production of a 62-PBq Cr-51 low-energy neutrino source for GALLEX*, *Nucl. Instrum. Meth. A* **378** (1996) 233.
- [36] V. Gavrin, *talk at the XXIX International Conference on Neutrino Physics, June 23, 2020*, .
- [37] P. Coloma, P. Huber and J.M. Link, *Combining dark matter detectors and electron-capture sources to hunt for new physics in the neutrino sector*, *JHEP* **11** (2014) 042 [[1406.4914](#)].
- [38] P. Coloma, P. Huber and J.M. Link, *Telling Solar Neutrinos from Solar Axions When You Can't Shut Off the Sun*, [2006.15767](#).
- [39] N. Vinyoles, A.M. Serenelli, F.L. Villante, S. Basu, J. Bergström, M. Gonzalez-Garcia et al., *A new Generation of Standard Solar Models*, *Astrophys. J.* **835** (2017) 202 [[1611.09867](#)].
- [40] J.N. Bahcall, A.M. Serenelli and S. Basu, *10,000 standard solar models: a Monte Carlo simulation*, *Astrophys. J. Suppl.* **165** (2006) 400 [[astro-ph/0511337](#)].
- [41] PARTICLE DATA GROUP collaboration, *Review of Particle Physics*, *PTEP* **2020** (2020) 083C01.
- [42] SAGE collaboration, *Measurement of the solar neutrino capture rate with gallium metal. III: Results for the 2002–2007 data-taking period*, *Phys. Rev. C* **80** (2009) 015807 [[0901.2200](#)].
- [43] BOREXINO collaboration, *First Simultaneous Precision Spectroscopy of pp , ${}^7\text{Be}$, and pep Solar Neutrinos with Borexino Phase-II*, *Phys. Rev. D* **100** (2019) 082004 [[1707.09279](#)].
- [44] BOREXINO collaboration, *The Monte Carlo simulation of the Borexino detector*, *J. Phys. Conf. Ser.* **1342** (2020) 012035.
- [45] BOREXINO collaboration, *Neutrinos from the primary proton–proton fusion process in the Sun*, *Nature* **512** (2014) 383.
- [46] V.V. Kuzminov and N.Y. Osetrova, *Precise measurement of C-14 beta spectrum by using a wall-less proportional counter*, *Phys. Atom. Nucl.* **63** (2000) 1292.
- [47] D. Foreman-Mackey, D.W. Hogg, D. Lang and J. Goodman, *emcee: The MCMC Hammer*, *Publ. Astron. Soc. Pac.* **125** (2013) 306 [[1202.3665](#)].
- [48] JUNO collaboration, *Neutrino Physics with JUNO*, *J. Phys. G* **43** (2016) 030401 [[1507.05613](#)].
- [49] A.N. Khan, $\sin^2 \theta_W$ *Estimate and Neutrino Electromagnetic Properties from Low-Energy Solar Data*, *J. Phys. G* **46** (2019) 035005 [[1709.02930](#)].
- [50] K. Mori, M. Kusakabe, A.B. Balantekin, T. Kajino and M.A. Famiano, *Enhancement of Lithium in Red Clump Stars by the Neutrino Magnetic Moment*, [2009.00293](#).
- [51] M. Smirnov, Z. Hu, J. Ling, Y. Novikov, Z. Wang and G. Yang, *Sterile neutrino oscillometry with Jinping*, *Eur. Phys. J. C* **80** (2020) 609 [[2002.05246](#)].

A Electron scattering signal distribution and the effective neutrino flux calculation for ${}^{51}\text{Cr}$ source

Outside source: We predict the signal event in different interfacial shell centered on the source with a radius R and a thickness dR as

$$N(R, t, T_e) = N_e(R) \sum_i \psi(R, t, E_i) \sum_{\alpha=e,\mu,\tau} P_{e\alpha}(E_i) \sigma_\alpha(E_i, T_e), \quad (\text{A.1})$$

where $N_e(R)$ is the total electron number density as a function of R in the shell, $\psi(R, t, E_i)$ is the neutrino flux as a function of radius R , time t and the i^{th} neutrino branch with different monoenergetic E_i . This formula can also be used for the light sterile neutrino study such as ref. [51]. In our case, there is almost no neutrino oscillation. Therefore, it can reduce to

$$N(R, t, T_e) = N_e(R) \sum_i \psi(R, t, E_i) \sigma_e(E_i, T_e), \quad (\text{A.2})$$

where, $N_e(R) = S(R) \rho_{\text{LS}} \rho_e N_{\text{A}}$ with the area of the shell $S(R)$ and $\psi(R, t, E_i) = f(E_i) \phi(R, t) = f(E_i) \frac{R_{51\text{Cr}}(t)}{4\pi R^2}$, in which $f(E_i)$ is the fraction of the i^{th} branch and $R_{51\text{Cr}}(t)$ is the decay rate initialized with 3 MCi. The area of the shell $S(R)$ is expressed by $S(R) = 2\pi \left(1 - \frac{(R_0+x)^2 + R^2 - R_0^2}{2(R_0+x)R}\right)$, where R_0 (~ 10.4 m) is the radius of the fiducial volume sphere and x (1 m) is the shortest distance from the source to the edge of the fiducial volume. So far, we obtain the total event number as a function of time t and T_e with the integral by R from x to $x + 2R_0$

$$N(t, T_e) = \frac{1}{2} \left[R_0 - \frac{(R_0+x)^2 - R_0^2}{2(R_0+x)} \ln \frac{x+2R_0}{x} \right] \rho_{\text{LS}} \rho_e N_{\text{A}} R_{51\text{Cr}}(t) \sum_i f(E_i) \sigma_e(E_i, T_e). \quad (\text{A.3})$$

If utilizing an effective ^{51}Cr decay rate $R_{51\text{Cr}}^{\text{eff}}$ during $T = 55$ days, it reduces to

$$N(T_e) = \frac{1}{2} \left[R_0 - \frac{(R_0+x)^2 - R_0^2}{2(R_0+x)} \ln \frac{x+2R_0}{x} \right] \rho_{\text{LS}} \rho_e N_{\text{A}} R_{51\text{Cr}}^{\text{eff}} T \sum_i f(E_i) \sigma_e(E_i, T_e), \quad (\text{A.4})$$

where $R_{51\text{Cr}}^{\text{eff}} = 6.005 \times 10^{16}$ Bq. Moreover, an effective neutrino flux ϕ_{eff} with respect to the whole fiducial volume can be written as $\phi_{\text{eff}} = \frac{3}{8\pi} \left[\frac{1}{R_0^2} - \frac{(R_0+x)^2 - R_0^2}{2(R_0+x)R_0^3} \ln \frac{x+2R_0}{x} \right] R_{51\text{Cr}}^{\text{eff}}$ so as to compare with the fluxes of solar neutrinos.

Inside source: With the same calculation strategy, the signal event in different spherical shell yields

$$N(R, t, T_e) = \rho_{\text{LS}} \rho_e N_{\text{A}} R_{51\text{Cr}}(t) \sum_i f(E_i) \sigma_e(E_i, T_e), \quad (\text{A.5})$$

which is an uniform distribution of R . With an integral by R and t , we obtain

$$N(T_e) = \rho_{\text{LS}} \rho_e N_{\text{A}} R_{51\text{Cr}}^{\text{eff}} (R_0 - r) T \sum_i f(E_i) \sigma_e(E_i, T_e), \quad (\text{A.6})$$

where r is the radius (0.5 m) of the sphere source shielding. In addition, we obtain an effective neutrino flux $\phi_{\text{eff}} = \frac{3}{4\pi(R_0^2 + rR_0 + r^2)} R_{51\text{Cr}}^{\text{eff}}$ to compare with the solar neutrino fluxes.

B An effective neutrino magnetic moment mixing $\mu_{\nu\tau}^{eff}$

We define an effective mixing of $\mu_{\nu\mu}$ and $\mu_{\nu\tau}$, $\mu_{\nu\mu\tau}^{eff}$. Therefore, (2.2) can be modified as

$$N_{pre} = N_e \sum_i \phi_i \int \int S_i^\odot(E) (P_{ee}^i(E) \sigma_e(E, T_e) + (P_{e\mu}^i(E) + P_{e\tau}^i(E)) \sigma_{\mu\tau}(E, T_e)) dE dT_e, \quad (\text{B.1})$$

with $\sigma_{\mu\tau} = \sigma_{\mu\tau}^{\text{SM}} + \sigma_{\mu\tau}^{\nu\mu\tau\text{MM}}$, and $\sigma_{\mu\tau}^{\nu\mu\tau\text{MM}} = \pi \frac{\alpha^2}{m_e^2} \left(\frac{\mu_{\nu\mu\tau}^{eff}}{\mu_B} \right)^2 \left(\frac{1}{T_e} - \frac{1}{E_\nu} \right)$. Moreover, remove the SM and $\nu_e\text{MM}$ contributions from the event number, resulting in

$$\begin{aligned} & \sum_i \phi_i \int \int \pi r_0^2 S_i^\odot(E) (P_{e\mu}^i(E) + P_{e\tau}^i(E)) (\mu_{\nu\mu\tau}^{eff})^2 \left(\frac{1}{T_e} - \frac{1}{E_\nu} \right) dE dT_e \\ &= \sum_i \phi_i \int \int \pi r_0^2 S_i^\odot(E) (P_{e\mu}^i(E) \mu_{\nu\mu}^2 + P_{e\tau}^i(E) \mu_{\nu\tau}^2) \left(\frac{1}{T_e} - \frac{1}{E_\nu} \right) dE dT_e, \end{aligned} \quad (\text{B.2})$$

where $\mu_{\nu\mu\tau}^{eff}$ can be split into $\mu_{\nu\mu}$ and $\mu_{\nu\tau}$. In this study, ${}^7\text{Be}$ (862 keV) dominates the proportions of $\mu_{\nu\mu}$ and $\mu_{\nu\tau}$ in $\mu_{\nu\mu\tau}^{eff}$ at ROI, the yellow band in figure 1. Therefore, (B.2) can reduce to

$$\left(P_{e\mu}^{7\text{Be}} + P_{e\tau}^{7\text{Be}} \right) \left(\mu_{\nu\mu\tau}^{eff} \right)^2 \simeq P_{e\mu}^{7\text{Be}} \mu_{\nu\mu}^2 + P_{e\tau}^{7\text{Be}} \mu_{\nu\tau}^2, \quad (\text{B.3})$$

where $P_{e\alpha}^{7\text{Be}}$ obeys (2.3). Further more, the average oscillation probability $P_{e\alpha}^{7\text{Be}}$ approximates $P_{e\alpha}(r = 0.06R_\odot, E = 862 \text{ keV})$, the probability from the densest point of ${}^7\text{Be}$ production in the sun to the earth. Therefore, we get $\left(\mu_{\nu\mu\tau}^{eff} \right)^2 \simeq 0.49 \mu_{\nu\mu}^2 + 0.51 \mu_{\nu\tau}^2$ with the neutrino oscillation parameters in ref. [41].